

## A Complete Monolithically-Integrated Circuit for All Optical Generation of Millimeter-Wave Frequencies

G. Allen Vawter, Alan Mar, Vincent M. Hietala, John Zolper and John Hohimer

Sandia National Laboratories  
Albuquerque, NM 87185-0603  
USA

### Abstract

The first monolithic integrated circuit for all-optical generation of millimeter wave signals is reported. The design integrates a mode-locked semiconductor ring diode laser with an optical amplifier and high-speed photodetector into a single optical integrated circuit. Signal generation is demonstrated at 30, 60 and 90 GHz frequencies.

### Key Words

Integrated optoelectronic circuits, mode locked lasers, semiconductor lasers, semiconductor optical amplifiers, ultrafast lasers.

### Introduction

Today, the generation of mm-wave signals typically uses discrete negative differential resistance diodes coupled to a metallic waveguide cavity resonant at the desired frequency. At frequencies near 100 GHz, the output power and efficiency of these sources is low (typically 10 mW output power and  $\leq 1\%$  efficiency); and higher frequencies are only accessible by frequency multiplying. Demonstration of passive mode-locking of semiconductor ring lasers at high pulse repetition rates<sup>1</sup> suggests the possibility of a photonic integrated circuit (PIC) comprising a mode-locked ring laser and traveling-wave photodiode<sup>2-4</sup> (TWPD) for direct generation of mm-wave electrical signals. Such a PIC could be much more compact and efficient compared to current technology and operate in the regime above 60 GHz where existing semiconductor-based mm-wave sources are inefficient or simply non-existent. In particular, Gunn diodes and IMPATT devices are limited to efficiencies of only a few percent. GaAs mm-wave integrated circuit (MMIC) oscillators are limited to roughly 5% and InP MMICs are limited to between 5 and 25% efficiency. Power output and efficiency of these devices drops rapidly above 100 GHz. By contrast a ring laser- and TWPD-based PIC

could eventually reach efficiencies up to 50% at frequencies above 100 GHz. In addition, such a PIC may be cleaved to separate the TWPD from the amplifier and an optical fiber used to transport the mm-wave power over large distances before conversion to mm-waves at the point of use.

We demonstrate the first monolithic PIC for generation of mm-wave signals. This new PIC integrates a passively mode-locked semiconductor ring laser, optical amplifier and high-speed photodiode for generation, amplification and detection of an optical pulse train with 30 to 90 GHz pulse-repetition frequency. Output is an electrical signal, generated by the photodiode, whose fundamental frequency is the pulse repetition rate of the mode-locked laser. The circuit uses a novel waveguide photodiode (WGPD) integrated with a mm-wave transmission line specifically designed for high-speed operation and signal extraction on a heavily-doped GaAs substrate.

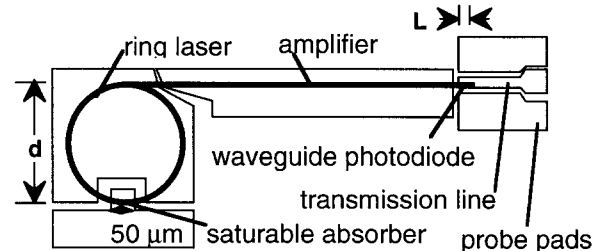


Figure 1. Schematic of actual mm-wave generation circuit.

The mm-wave signal generation PIC design for 60 and 90 GHz signals is shown in Fig. 1. A closed-ring GaAs/AlGaAs diode laser with a separately contacted, reverse-biased saturable absorber is passively mode locked generating a continuous train of short (1 to 10 ps) optical pulses in the ring cavity. Output of the ring laser is coupled to optical waveguide amplifier using a multi-mode Y-junction. A direct-waveguide photodetector (WGPD) converts the optical pulse train emerging from the amplifier to a mm-wave electrical output. Finally, a 50-Ohm transmission line is integrated with the WGPD for removal

of the electrical signal. A WGPD was chosen rather than a velocity-matched TWPD so that the PIC requires only one epitaxial growth sequence. The pn-junction design is optimized for laser and amplifier operation and does not have a large enough depletion width to accommodate a velocity-matched photodetector. An alternate configuration was used for 30 GHz signals wherein the reverse-biased saturable absorber also functions as a high-speed photodetector, converting a fraction the lasing pulse train into a mm-wave electrical output. Although more simple, this configuration does not offer the output power potential of the PIC using an optical amplifier and WGPD.

**Design**

The pulse repetition frequency,  $f$ , of the mode-locked laser is fixed by the cavity round trip time which is determined by the diameter of the ring according to (1)

$$f = \frac{c}{n_{eff}} \times \frac{1}{\pi d} \tag{1}$$

where  $c$  is the vacuum speed of light,  $n_{eff}$  the group effective refractive index of the multimode ring waveguide and  $d$  the ring diameter. Using the known 86 GHz rate for a 300  $\mu\text{m}$  ring employing 6- $\mu\text{m}$  wide multilateral-moded rib waveguides, rings of nominally 30, 60 and 90 GHz pulse-repetition frequency were designed having diameters of 860, 430 and 290  $\mu\text{m}$  respectively. Light output from the ring laser is coupled by an equal-width branching Y-junction into a 1-mm long waveguide optical amplifier providing optical gain to the pulse train prior to coupling into the WGPD. Fig. 2 shows cross sections of the four circuit elements.

The WGPD was designed for high-speed operation and minimum capacitive loading caused by the n-type doped substrate. The WGPD, Fig. 2b, has a small active area and is coupled directly into a 50 Ohm transmission line, Fig. 2c, and ground-signal-ground contact pads. Dimensions of the transmission line were selected to give low loss and 50 Ohm characteristic impedance. The WGPD is fabricated by inserting the pn-junction waveguide material between the center electrode and ground plane of the transmission line. The additional loss and capacitance of the diode lowers the characteristic impedance and raises the effective refractive index sufficiently that device lengths below 200  $\mu\text{m}$  are adequately viewed as lumped photodiodes. Both 10 and 80  $\mu\text{m}$  WGPD lengths were integrated with the 60 and 90 GHz lasers. All detectors are 6  $\mu\text{m}$  wide, matching the width of the laser and amplifier waveguides. Calculated optical absorption within the waveguide due to the reverse-biased quantum well is 430 dB/cm. At this absorption level 10% of the light intensity will be absorbed by the photodiode in 10  $\mu\text{m}$  of waveguide length and 55% in 80  $\mu\text{m}$ . These values are the upper limit of WGPD efficiency. The end of the WGPD was etched at an angle<sup>5</sup> to suppress reflections and feedback to the ring laser.

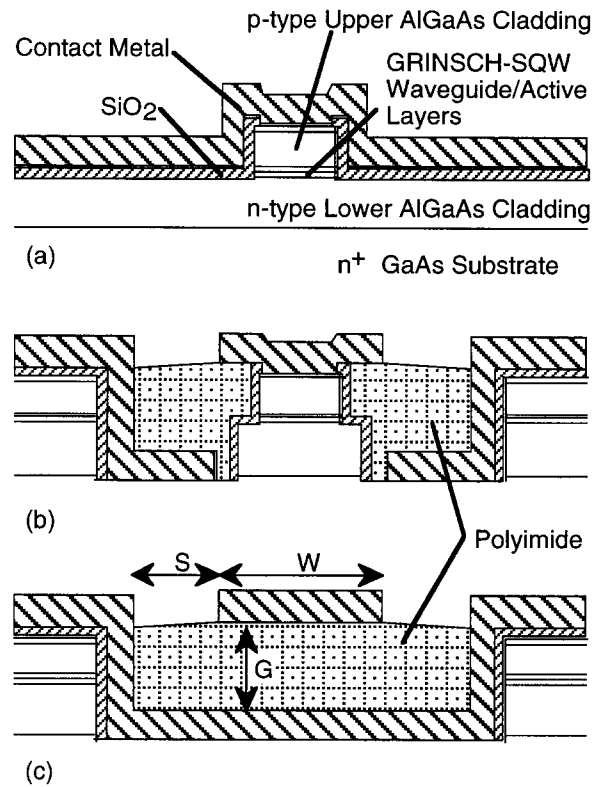


Figure 2. Cross-section views of the three principle circuit elements comprising the all-optical mm-wave signal generator. (a) Laser and amplifier active waveguide. (b) Waveguide photodiode. (c) Millimeter-wave transmission line. Key dimensions are:  $W = 12 \mu\text{m}$ ,  $S = 5 \mu\text{m}$  and  $G = 10 \mu\text{m}$ .

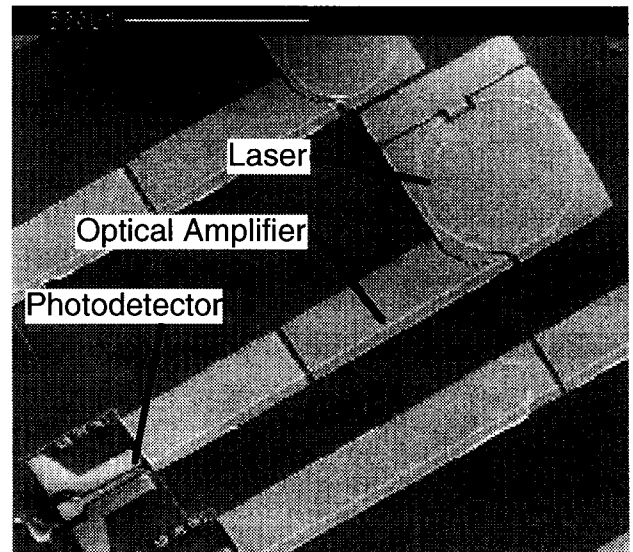


Figure 3. Electron micrograph view of complete all-optical mm-wave signal generation PIC. Total length of the circuit is less than 2 mm.

## Fabrication

The epitaxial structure for our mm-wave generation OEIC is a single-quantum-well (10 nm) graded index separate-confinement-heterostructure in GaAs/Al<sub>x</sub>Ga<sub>1-x</sub>As with  $x=0.6$  cladding layers. Overall thickness of the undoped graded layers and quantum well is 0.41  $\mu\text{m}$ . Oxygen ion implantation of the p-type layers in the regions between circuit elements was used to provide electrical isolation. The implant was annealed at 850°C for 30 s to recover optical transparency while maintaining high-resistivity.<sup>6, 7</sup> The 6- $\mu\text{m}$  wide laser, output coupler, amplifier and WGPD multilateral mode rib waveguides were formed simultaneously by chlorine reactive ion beam etching (RIBE) through the active layer. The deep trench for the WGPD and transmission line was formed in a second RIBE step. WGPD n-type ohmic contacts and transmission line ground plane metalization were deposited in the trench followed by a polyimide dielectric used to support the p-type WGPD contact and transmission line center electrode. The laser, amplifier and WGPD p-type ohmic contacts and transmission-line center electrode were deposited in a single step. Completed PICs were tested p-side up without heat sinking. Fig. 3 is an SEM image of a complete PIC. Although the straight amplifier section is broken into two separately contacted sections, all data presented here was taken by shorting the two sections together and applying a common bias current.

Table 1. Operating currents and voltages for selected mm-wave generation PICs.

Ring Dia. ( $\mu\text{m}$ )	Ring Current (mA)	Absorber Bias (V)	Amp. Current (mA)	WGPD Bias (V)
860	130	-2.9	70	-2.9
430	180	-3.3	70	-18
290	192	-3.4	70	-17

## Results

Millimeter-wave output of PICs was measured using DC bias currents to the ring laser and amplifier. Mode-locking of the ring laser was established by reverse biasing the saturable absorber while monitoring the WGPD using Cascade co-planar probes and an HP8565E spectrum analyzer. Harmonic mixers were used at the input of the spectrum analyzer for heterodyne detection of frequencies above 50 GHz. Table 1 details the required bias conditions of the three ring diameters for stable mode-locking.

Output frequency, power is plotted in Fig. 4. Measured output power and frequency of the 860, 430 and 290  $\mu\text{m}$  diameter of rings were -12 dBm at 29.1 GHz, -23

dBm at 57.5 GHz and -27 dBm 85.2 GHz respectively. Frequency generation close to the desired value was achieved for all three laser diameters. The signals have a typical linewidth of 0.3 - 1.0 MHz, influenced primarily by timing jitter of the pulse train. This jitter was determined by integrating the sideband noise and ranged from about 0.3 - 1.0 ns RMS, such values are not unusual for passively mode-locked semiconductor lasers.

Gain of the optical amplifier was measured in the range of 3 to 4 dB per 0.5 mm amplifier segment under CW operation. Data was taken using the same bias currents indicated in Table 1. At a fixed laser drive current, gain of an individual amplifier section is determined by the ratio of photocurrents measured using the first amplifier stage in reverse bias and then forward biasing the first amplifier stage while using the second stage in reverse bias. Since intra-band carrier relaxation times are similar to the mode-locked pulse length, measurement of CW gain is an approximation of the actual gain under mode-locked operation.

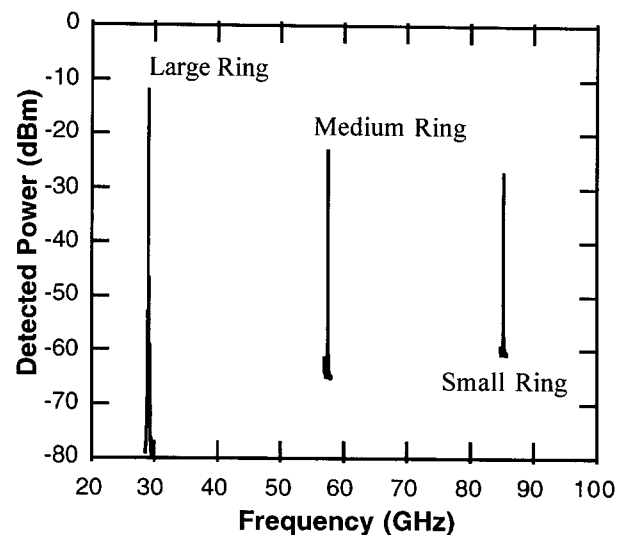


Figure 4. Measured performance of three different mm-wave signal generation PICs. Large, medium and small rings are 860, 430 and 290  $\mu\text{m}$  diameter respectively.

## Discussion

The output frequency of our PIC is well described by (1). Cavity frequencies are approximately 5% below the predicted values, this error is dominated by variation of  $n_{\text{eff}}$  from the ideal. Output power of these first demonstration PICs is limited by WGPD efficiency. By comparison, optical autocorrelation measurements of pulse output of cleaved ring lasers have shown up to 0 dBm average power output at 87 GHz repetition rate.<sup>1</sup> Direct measurement of relative response of WGPDs separated from PICs shows a 20 dB roll-off at 40 GHz. WGPD performance may be limited by factors such as contact resistance, incomplete

absorption within the device, and RF losses within the metal and polyimide. Considering the WGPD response of no better than -20 dB and approximately 6 dB gain available from the optical amplifier, our integrated ring lasers appear to be generating average output power similar to the earlier discrete devices.

Output power of the mm-wave PIC is influenced by a number of factors including the internal circulating power of the ring, the amount of power coupled out of the ring, gain of the amplifier and the efficiency of the photodiode. All of these require optimization to extract the maximum mm-wave power. Power extraction from the laser could be improved through use of reflective facet output couplers<sup>8</sup> in place of Y-junctions, thereby improving control of the ratio of output-coupled power to circulating power. Wider pulses, up to a duty cycle of approximately 50%, could improve the output power at the fundamental frequency by as much as 10 dB. Such pulse broadening may be achievable using grating or waveguide-coupler filters within the ring cavity to reduce the lasing spectral bandwidth. Improvements in amplifier gain, detector efficiency and detector power handling capability would also increase the output power of the PIC. Use of a TWPD would increase the output by as much as a factor of 10 at these demonstration frequencies and may be required above 100 GHz due to the poor WGPD efficiency. A flared amplifier with one or more photodiodes operating in parallel at the wide amplifier output end may result in dramatic power enhancements. Finally, pulse-to-pulse timing jitter could be reduced to the femtosecond regime through the use of an electronic phase-lock loop providing feedback from the pulse output to the saturable absorber section.

## Conclusion

In summary, we have demonstrated the first PIC for direct generation of mm-wave frequencies. This PIC integrates a passively mode-locked semiconductor ring laser with an optical amplifier and high-speed waveguide photodiode. By generating and amplifying a train of optical pulses and using an integrated waveguide photodiode to convert the optical pulses into an electrical signal, this circuit has been used to generate -23 and -27 dBm of mm-wave power at 57.5 and 85.2 GHz respectively. Similarly, direct sampling of the saturable absorber has generated -12 dBm at 29.1 GHz. PICs using this concept can be used in a wide variety of applications where a very compact, lightweight mm-wave source is required.

## Acknowledgments

The authors would like to thank D. Tibbetts-Russell, B. Fuchs for technical assistance. This work was supported by United States Department of Energy under Contract DE-AC04-94AL85000. Sandia is a multiprogram laboratory operated by Sandia Corporation, a

Lockheed-Martin Company, for the United States Department of Energy.

## References

- [1] J. P. Hohimer and G. A. Vawter, "Passive mode locking of monolithic semiconductor ring lasers at 86 GHz," *Appl. Phys. Lett.*, vol. 63, pp. 1598-1600, 1993.
- [2] V. M. Hietala, G. A. Vawter, T. M. Brennan and B. E. Hammons, "Traveling-wave photodetectors for high-power large-bandwidth applications," *IEEE Trans. on Microwave Th. and Tech.*, vol. 43, pp. 2291-2297, 1995.
- [3] K. S. Giboney, R. L. Nagarajan, T. E. Reynolds, S. T. Allen, R. P. Mirin, M. J. Rodwell and J. E. Bowers, "Travelling-wave photodetectors with 172-GHz bandwidth and 76 GHz bandwidth-efficiency product," *IEEE Phot. Technol. Lett.*, vol. 7, pp. 412-414, 1995.
- [4] L. Y. Lin, M. C. Wu, T. Itoh, T. A. Vang, R. E. Muller, D. L. Sivco and A. Y. Cho, "Velocity-Matched Distributed Photodetectors with High-Saturation power and large bandwidth," *IEEE Phot. Technol. Lett.*, vol. 8, pp. 1376-1378, 1996.
- [5] J. P. Hohimer, G. A. Vawter, D. C. Craft and G. R. Hadley, "Improving the Performance of Ring Diode Lasers by Controlled Reflection Feedback," *Appl. Phys. Lett.*, vol. 61, pp. 1013-1015, 1992.
- [6] J. C. Zolper, A. G. Baca and S. A. Chalmers, "Thermally Stable Oxygen Implant Isolation of p-type AlGaAs," *Appl. Phys. Lett.*, vol. 62, pp. 2536-2538, 1993.
- [7] R. P. Bryan, J. J. Coleman, L. M. Miller, M. E. Givens, R. S. Averback and J. L. Klatt, "Impurity induced disordered quantum well heterostructure stripe geometry lasers by MeV oxygen implantation," *Appl. Phys. Lett.*, vol. 55, pp. 94-96, 1989.
- [8] J. P. Hohimer, G. R. Hadley and G. A. Vawter, "Semiconductor Ring Lasers With Reflection Output Couplers," *Appl. Phys. Lett.*, vol. 63, pp. 278-280, 1993.